ACS APPLIED NANO MATERIALS

www.acsanm.org Article

Sub-nm Pore Size of Phenylethynyl End-Capped Imide Oligomer-Derived Carbon for Molecular Sorption and Separation

William Guzman, Anthony Griffin, Mark Robertson, William L. Jarrett, Zhe Qiang, and Jeffrey S. Wiggins*

Cite This: *ACS Appl. Nano Mater.* 2023, 6, 14957−14966 Read Online

ACCESS | Metrics & More | Article Recommendations | Supporting Information

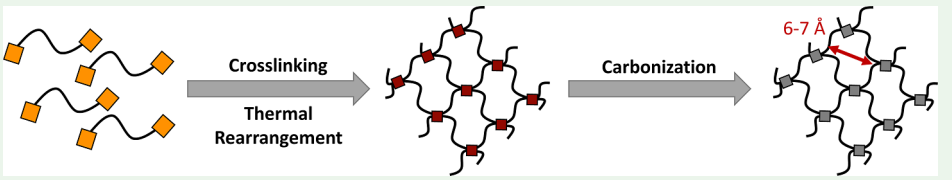

ABSTRACT: Carbon molecular sieves (CMSs) derived from polymer precursors that can be prepared at scale are attractive for various energy-efficient sorption and separation technologies, such as hydrogen recovery, air purification, and hydrocarbon separation. Preparing CMSs with uniform sub-nm pores is prudent but rarely studied. Here, we report the use of phenylethynyl-terminated crosslinkers to control pore size, leading to highly uniform pore formation between 6 and 7 Å. We demonstrate that incorporating phenylethynyl-terminated functionalities into thermally rearrangeable (TR) imide oligomers with asymmetric chemical structures results in CMSs with consistent pore sizes (6−7 Å), high surface areas (up to 775 m^2/g), and excellent CO_2 sorption performance (3.17 mmol CO_2/g of CMS). Additionally, our results indicate that sub-nm pore formation can be further tailored through polymer network architecture, leading to variable surface areas (569−735 m^2/g), which is accomplished through composition control of polymer precursors with and without TR capabilities. The fundamental understandings about the impact of the molecular design of phenylethynyl-terminated polymer precursors on their derived carbon structure can provide critical insights into their rational design for future molecular sorption and separation applications.

KEYWORDS: *carbon molecular sieves, uniform sub-nm pores, molecular design, polymer network architecture*

INTRODUCTION

Carbon molecular sieves (CMSs) have attracted much attention in recent years due to their great potential in the development of next-generation separation technologies for gases and liquids, which account for 10−15% of the global energy consumption.[1−3] Specifically, membrane-based separations can lead to an order of magnitude improvement in energy efficiency compared to conventional thermal-based processes.[3−5] Molecular sieving separation enabled by CMSs is controlled via thermodynamic partitioning and diffusion kinetics, which provides opportunities for complementary molecular diffusion and sorption selectivity through CMS engineering, such as developing uniform pore channels and heteroatom doping of the carbon framework.[6] However, fabrication of ordered sub-nm porous structures in carbonaceous materials remains challenging, as uncontrollable defect formation that occurs during the carbonization step can cause a broad pore size distribution (PSD) below 1 nm.[7]

Several examples of ordered sub-nm porous CMSs have been previously reported through carbonization of bamboo, oil-tea shells, cacti, and camphor seed husks with ionic salts such as KOH or K_2CO_3.[8−11] Similar methods have also been demonstrated for preparing sub-nm porous CMSs by carbonizing metal organic frameworks (MOFs) with KOH.[12] Despite their great properties, removal of ionic salts from carbonized materials requires additional washing steps, thus increasing synthesis complexity. Therefore, several researchers have investigated strategies of direct pyrolysis of covalent organic frameworks (COFs),[13,14] porous organic frameworks,[15] zeolitic imidazolate frameworks,[16] and MOFs,[17] resulting in uniform sub-nm porous CMSs. However, scale-up of these materials remains challenging due to their associated high costs.[15,17]

Amorphous CMSs can also be prepared using polymer precursors, which usually contain bimodal PSD comprising micropores (7−20 Å) and ultramicropores (<7 Å), while monomodal PSD in a sub-nm range is still difficult to achieve and underexplored.[18,19] Specifically, while many works have focused on the development of hierarchical porosity (combining micro-, meso-, and macropores) in CMSs, limited studies have demonstrated effective pore engineering at sizes

Received: June 5, 2023
Accepted: July 28, 2023
Published: August 15, 2023

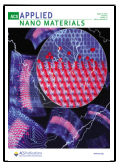

https://doi.org/10.1021/acsanm.3c02516
ACS Appl. Nano Mater. 2023, 6, 14957−14966

<10 Å through rational polymer precursor molecular design.[12,20−22] A recent report by Du and coworkers showed that thermally controlled pyrolysis of polydopamine can achieve micropores between 4.7 and 5.3 Å, elucidating the importance of matching the CMS pore size to the kinetic diameter of the gas molecule of interest for molecular separations.[7] Koh et al. reported that carbonization of crosslinked poly(vinylidene fluoride) can result in a CMS with well-defined bimodal pore sizes of 6−7 and 8−9 Å, respectively.[23] Notably, pore sizes between 6 and 9 Å could efficiently separate liquid xylene isomers that typically require energy-intensive separation, such as through crystallization and simulated moving bed adsorption,[24,25] without pore swelling or PSD changes.[23,26,27] We note that few literature examples can be found associated with the direct carbonization of polymers to prepare CMSs with separation capabilities containing well-defined, sub-nm pore sizes,[7,19,27] which may be due to the underdevelopment of the polymer precursor molecular design. Addressing this technology gap would further advance the synthetic capabilities of polymer-derived CMS while expanding their application domains for gas and liquid sorption and separation.

Ortho-hydroxyl polyimides can undergo thermal rearrangement (TR) to form polybenzoxazoles (PBOs) with intrinsic microporosity,[28−30] which generally have characteristic bimodal pore sizes around 4 and 8 Å.[30−34] However, Do and coworkers demonstrated that monomodal sub-nm pore sizes can be prepared through TR of a crosslinked bismaleimide (BMI) monomer precursor,[35] which is attributed to the synergistic effects of the TR process and highly crosslinked nature of the BMI network. In this work, end-capped maleimide crosslinkers can promote pore size control during the TR process through limiting the length of the polymer backbone. Furthermore, the well-defined pore size (∼7.3 Å) could be maintained upon carbonization of the crosslinked network, which has been previously demonstrated by Koh and coworkers from using crosslinked poly(vinylidene fluoride).[23] To further develop and build on these seminal works, there is a strong need to study and enable PSD control from direct carbonization of end-capped crosslinking TR polymer networks.

Phenylethynyl-terminated imide (PETI) oligomers and their derived polymer networks are broadly employed in high-temperature polymer composite applications in the aerospace industry.[36−42] PETI-type oligomers undergo crosslinking through radical polymerization at elevated temperatures (325−400 °C), forming linear acetylenic structures at lower temperatures around 325 °C and crosslinked cyclized rings at temperatures greater than 350 °C.[43−48] Recent studies have incorporated ortho-hydroxyl functionalities into the backbone of PETI imide oligomers, enabling TR during network formation.[49−51] TR conversion and the resulting film properties such as dielectric constant, glass transition temperature (T_g), and thermal degradation of the crosslinked TR-PBO networks (TR-PBOx) were elucidated, while their pore structures and properties remain less understood.

This work focuses on end-cap crosslinking and carbonization of TR-PBOx for preparing CMS materials with controlled microporosity development for molecular sorption and separation applications. Phenylethynyl-terminated *ortho*-hydroxy imide oligomers (oHIOs) were synthesized via a two-step azeotropic imidization method. oHIO powders were crosslinked, undergoing TR between 350 and 450 °C in an inert atmosphere and leading to the formation of TR-PBOx, which were subsequently carbonized up to 800 °C. We demonstrated that the oHIO degree of polymerization (DP) as well as the fractional free volume (FFV) of TR-PBOx play a significant role in impacting the micropore size and surface areas of their derived CMSs. Furthermore, the heteroatom content and microporous carbon structure of CMSs are investigated. These heteroatom-doped porous carbons with controlled pore size can profoundly influence future molecular sieving applications in gas and liquid sorption and separation technologies.

EXPERIMENTAL SECTION

Materials. Toluene (99.85%) and anhydrous *N*-methyl-pyrrolidone (NMP) (>99.5%), were purchased from Fisher Scientific. 1,3′-Bis (3-aminophenoxy)benzene (APB-133, 99%) was purchased from Chriskev Incorporated. 2,2-Bis(3-amino-4-hydroxyphenyl)-hexafluoropropane (6FAP, 99%) was obtained from Alfa Chemistry. 2,3,3′,4′-Benzophenone dianhydride (*a*-BTDA, 99%) was received from Jayhawk Fine Chemicals Corp., part of CABB Group GmbH. 4-(Phenylethynyl)phthalic anhydride (PEPA, 99%) was received from Nexam Chemical. Deionized H_2O was obtained in-house from the University of Southern Mississippi. All materials were used as received unless otherwise noted.

***o*-Hydroxy Imide Oligomers Synthesis.** *o*-Hydroxy imide oligomers (oHIOs) with target DPs of 4, 8, and 12, corresponding to number-average molecular weights (M_n) of approximately 2500, 5000, and 9000 g/mol, were prepared following a previously reported method.[49] In brief, for a target DP of 8, a 250 mL two-neck flask equipped with a Dean−Stark trap and a reflux condenser was charged with a solution of 6FAP (36 mmol) in NMP (59 mL), and then a-BTDA (32 mmol) was slowly added. The mixture was stirred for 1 h at room temperature until fully dissolved before the PEPA end-capper (8 mmol) was slowly introduced to the reaction solution and stirred for 16 h under N_2. The reaction solution was then charged with toluene (60 mL) before heating at 180 °C for 16 h. The reaction solution was cooled to room temperature, precipitated into deionized H_2O, and dried at 250 °C for 6 h in a vacuum oven. oHIO monomers were named according to the target DP and stoichiometrically controlled by adjusting the molar ratio between 6FAP, a-BTDA, and PEPA. For example, oHIO-4 refers to an oHIO sample with a target DP of 4. A non-TR IO control was synthesized using a similar protocol with a target DP of 4 (M_n of 2500 g/mol). A more detailed synthetic procedure can be found in the Supporting Information.

Thermally Rearranged Crosslinked Polybenzoxazole Film Preparation. oHIO powders were transferred to an UPILEX-S film template (obtained from UBE Corporation) on steel plates and then bagged using a high-temperature Thermalimide (obtained from Airtech International Inc.) film equipped with a vacuum port (Figure S1). Thermally rearranged crosslinked polybenzoxazole (TR-PBOx) films were pressed under vacuum through a stepwise curing process, heating at 300 °C for 0.5 h and 400 °C for 1 h in a Carver press under a pressure of 5000 psi. TR-PBOx films were cooled to room temperature before being removed from the Thermalimide bag.

CMS Preparation. oHIO powders were transferred to a tube furnace and heated from room temperature to 350 °C at a ramp rate of 5 °C/min and isothermally held at 350 °C for 2 h, enabling crosslinking of PEPA functionalities. Samples were then heated from 350 to 450 °C at a heating rate of 5 °C/min and isothermally held at 450 °C for 1 h to form TR-PBOx. These networks were named according to the target DP from synthesis. For example, TR-PBOx-4 would indicate the thermally treated oHIO sample with a target DP of 4. TR-PBOx networks were then heated from 450 to 800 °C at a heating rate of 1 °C/min under constant N_2 flow (300 mL/min) during the carbonization process. The derived carbonaceous samples were named according to the target DP from synthesis. For example, CMS-4 would indicate a thermally treated and carbonized oHIO

https://doi.org/10.1021/acsanm.3c02516
ACS Appl. Nano Mater. 2023, 6, 14957−14966

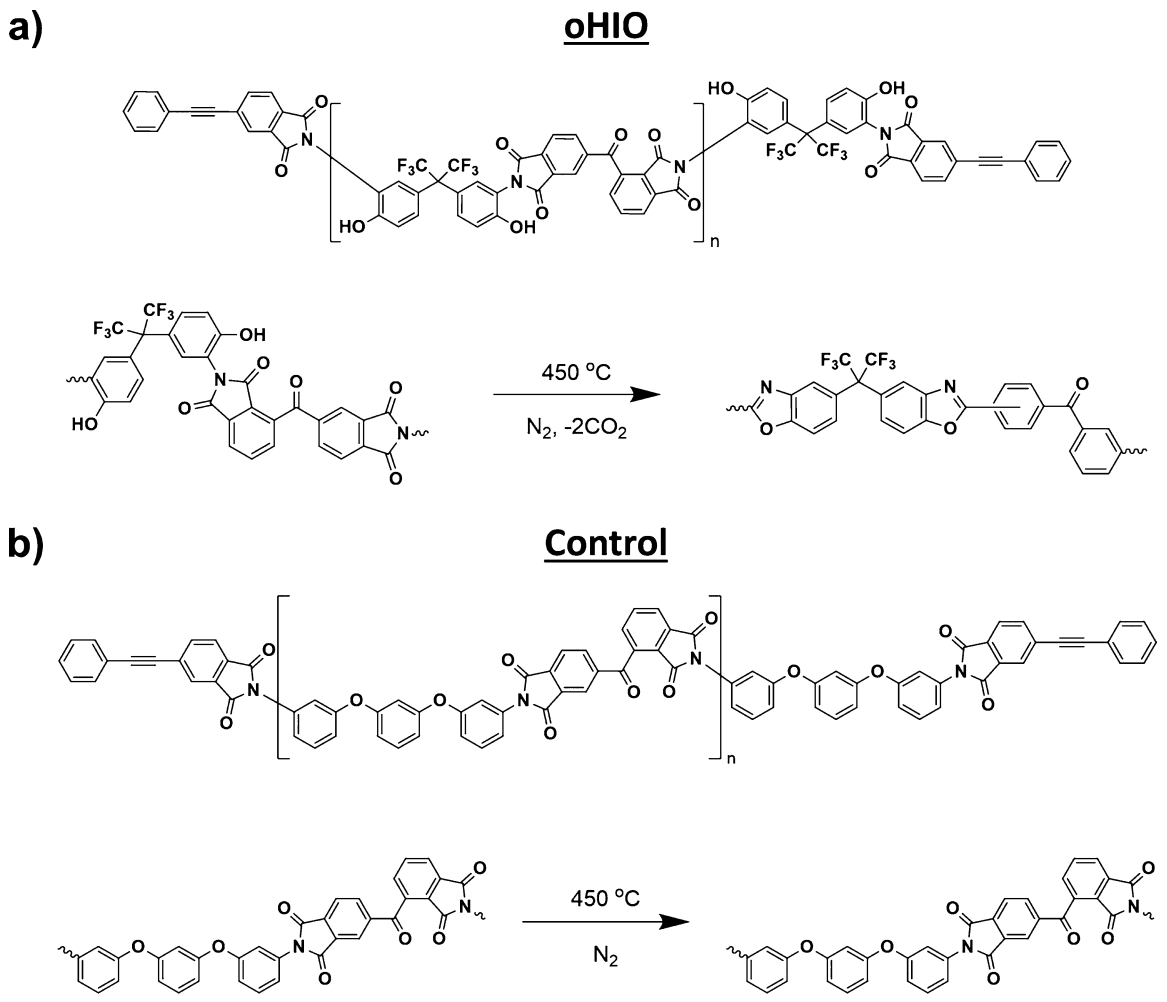

Figure 1. (a) Chemical structure of the oHIO samples with change in the chain topology after curing and TR at 450 °C. (b) Chemical structure of the control with no change in the chain topology following a cure at 450 °C.

sample with a target DP of 4. The CMS derived from the control is referred to as CMS-*c*, hereafter.

Characterization Methods. ^{1}H nuclear magnetic resonance (NMR) spectroscopy measurements were conducted using a Bruker Ascend 600 spectrometer (Bruker Corporation, Billerica, Massachusetts, USA) at a 600 MHz proton frequency and temperature of 303 K. All samples were dissolved in deuterated dimethyl sulfoxide (DMSO-d_6) at a concentration of 40 mg/mL for ^{1}H NMR characterization. ^{13}C solid-state cross polarization magic angle spinning (CP-MAS) NMR spectroscopy was performed on a Varian UNITY-INOVA 400 MHz spectrometer (Varian Inc., Palo Alto, CA, USA) using a Chemagnetics three-channel 4 mm PENCIL-style probe. Samples were loaded into zirconia rotor sleeves, sealed with Teflon caps, and spun at rate of 10.0 kHz. CP/MAS[52] was used with high-power proton decoupling implemented during data acquisition. The acquisition parameters were as follows: the ^{1}H 90° pulse width was 6.675 μs, the dead time delay prior to data acquisition was 6.4 μs, and the acquisition time was 45 ms. The cross polarization time was either 4 ms (for TR-PBOx samples) or 5 ms (for oHIO and the IO control precursor samples), with the ^{13}C RF field linearly ramped from 35.4 to 39.4 kHz.[53] A recycle delay of 3 (TR-PBOx) or 5 s (oHIO and the IO control samples) between scans was utilized, and a ^{1}H decoupling field of 37.5 kHz was implemented during acquisition. The number of co-added scans varied from 1856 to 6336.

The number average molecular weight (M_n), weight average molecular weight (M_w), and dispersity ($Đ$) were determined by gel permeation chromatography (GPC) relative to polystyrene standards at 45 °C in tetrahydrofuran (THF) using a Waters ACQUITY Advanced Polymer Chromatography system configured with ACQUITY APC XT 450, ACQUITY APC XT 125, and APC XT 45 columns in series. PETI oligomer samples were pre-dissolved at a concentration of 1.00−2.00 mg/mL in THF with stirring at 45 °C for 1 h. Thermal gravimetric analysis coupled with simultaneous mass spectrometry (TGA−MS) characterization experiments were performed on a TA Instruments Discovery Series TGA with a Discovery MS (TA Instruments, New Castle, Delaware, USA), which was operated between 100 and 1000 °C at a 10 °C/min heating rate, under a continuous flow of N_2 at 10 mL/min. The ion current (mA) was measured for atomic mass units (amus) of H_2O (18 amu), HF (20 amu), CO_2 (44 amu), and COF_3 (85 amu) using the peak jump data collection method. Attenuated total reflectance Fourier transform infrared (ATR−FTIR) spectroscopy was carried out on a PerkinElmer Frontier spectrometer with the scanning wavenumber in the range of 4000−600 cm^{-1} at a resolution of 2.0 cm^{-1} (PerkinElmer Inc., Waltham, Massachusetts, USA).

A Micromeritics Tristar II instrument was used to determine the CMS pore texture, including their adsorption and desorption isotherms under N_2 at 77 K. The surface area was determined using Brunauer−Emmett−Teller (BET) analysis, and the PSD was calculated using the Horvath−Kawazoe (HK) model, assuming a slit-pore geometry for final CMS samples. Additionally, this instrument was also utilized to determine the CO_2 sorption performance of CMS samples at 293 K by measuring their respective sorption isotherms from 0.01 to 1 bar.

Wide-angle X-ray scattering (WAXS) experiments were conducted on a laboratory beamline system (Xenocs Inc. Xeuss 2.0) with an X-

https://doi.org/10.1021/acsanm.3c02516
ACS Appl. Nano Mater. 2023, 6, 14957−14966

ray wavelength of 1.54 Å and a sample to detector distance of 150.8 mm. Samples were kept under vacuum to minimize the background of air scattering. WAXS data reduction and analysis were performed using Nika software, and correlation spacing (d) was calculated using Bragg's law, where Q is the scattering vector (eq 1).

$$Q = \frac{2\pi}{d} \tag{1}$$

X-ray photoelectron spectroscopy (XPS) characterization was performed on a Thermo Fisher ESCALAB Xi + spectrometer equipped with a monochromatic Al X-ray source (1486.6 eV) and a MAGCIS Ar+/Ar_n+ gas cluster ion sputter gun. Measurements were performed using the standard magnetic lens mode and charge compensation. The base pressure in the analysis chamber during spectral acquisition was at 3×10^{-7} mbar. The pass energy of the analyzer was set to 20 eV for high-resolution spectra and 150 eV for survey scans, with energy resolutions of 0.1 and 1.0 eV, respectively. An average of five scans were completed for high-resolution spectra and two scans were completed for survey spectra. Binding energies were calibrated with respect to the C1s peak at 284.8 eV. Thermo Scientific Avantage analysis software v5.9904 was used to analyze the heteroatom content of CMS carbon samples.

Densities of crosslinked films were measured in DI water at ambient temperature with an analytical balance (ML204 Mettler Toledo) combined with a density kit using dry films by the Archimedes principle. FFV was calculated from the experimentally determined density according to previously published literature (eq 2).[54,55]

$$\mathrm{FFV} = \frac{V - V_o}{V} \tag{2}$$

The specific volume (V) of the polymer network is calculated from the experimentally determined density, and the occupied volume (V_o) is estimated by Bondi's group contribution method using eq 3

$$V_o = 1.3 \sum V_{vdW} \tag{3}$$

where V_{vdW} is the van der Waals volume of a single repeating unit and the fraction of the end groups according to their calculated molecular weights.

RESULTS AND DISCUSSION

CMS Formation via the oHIO Precursor. A two-step process was used to prepare a series of CMSs from PEPA end-capped, oHIO precursors with varying DP (Figure 1a). oHIO precursors were first synthesized via azeotropic imidization reactions, stoichiometrically controlling DP according to an established method (Table S1).[56] A PEPA end-capped IO (control) that cannot undergo TR was synthesized using a similar procedure (Figure 1b). oHIO and IO precursor structures were confirmed via solution-state ^{1}H NMR, where hydroxyl functionalities were observed in the oHIO precursors at a chemical shift of 10.4 ppm (Figure S2).

oHIO and IO precursors were then placed into a tube furnace for crosslinking of phenylethynyl groups at 350 °C for 2 h, similar to previous literature.[36,37] Crosslinked oHIO precursors were then isothermally held at 450 °C for 1 h, resulting in TR-PBOx formation. Particularly, a TR temperature of 450 °C was selected based on the TGA results (Figure 2a), which can lead to complete oHIO TR without thermal degradation. TGA–MS characterization was conducted to determine the completion of oHIO TR via CO_2 detection (Figure S3). Additionally, crosslinking and TR were confirmed via ATR–FTIR through alkyne peak disappearance (2215 cm^{-1}) and new benzoxazole ring formation bands at 1478 and 1056 cm^{-1} (Figure 2b).[50,51,57]

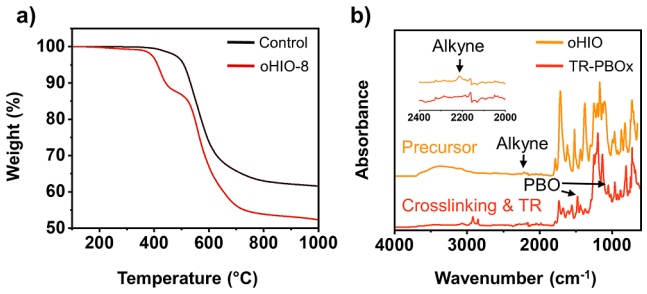

Figure 2. (a) Example TGA weight loss vs temperature of oHIO-8 and the IO control samples showing distinct TR weight loss in oHIO-8 and char yields for both samples. (b) ATR–FTIR spectra of the precursor with an alkyne crosslinker band at 2215 cm^{-1} and PBO ring formation stretches following crosslinking and TR.

Asymmetric/symmetric imide carbonyl (1783/1714 cm^{-1}) and hydroxyl (3700–3200 cm^{-1}) ATR–FTIR bands were drastically reduced after crosslinking and TR, further indicating oHIO conversion into TR-PBOx.[29,30] Additionally, the completion of TR was confirmed using ^{13}C solid-state CP-MAS NMR, wherein chemical shifts of the benzoxazole ring in the TR-PBOx samples were observed at 163, 150, and 141 ppm, similar to previous reports (Figures S4–S6).[29,50,51,58] However, the chemical shifts at 192, 165, 158, 132, and 122 ppm observed in the control remained the same following thermal annealing at 350 and 450 °C, thus signifying that no TR occurred in the control (Figure S7).

It has been previously demonstrated that pyrolysis of linear *ortho*-hydroxy polyimide precursors at temperature up to 800 °C yielded nitrogen-doped CMSs.[59–61] In this work, TR-PBOx networks were carbonized at 1 °C/min from 450 to 800 °C to form CMSs, which was confirmed via ATR–FTIR (Figure S8). A monolithic morphology with particle sizes of ∼300 and ∼50 μm was observed for the control (CMS-*c*) and CMS-8, respectively, using scanning electron microscopy (SEM) (Figure S9).

XPS characterization was performed to investigate the heteroatom content present in the CMS following TR-PBOx carbonization up to 800 °C (Figure 3). As previously discussed, incorporation of heteroatoms, such as nitrogen and oxygen, into CMS materials provide advantages to improve their physicochemical properties, altering charge density and electronegativity, which can enable enhanced charge transfer or chemical interactions for many applications, such as molecular sieving.[59,62] XPS survey scans indicated the presence of C, O, and N heteroatoms in CMS samples following TR-PBOx precursor carbonization (Figure 3a and Table S2). High-resolution XPS spectra were used to further elucidate the chemical environment of the atoms found in the CMS (Figures 3b–d and S10–S12). As an example, CMS-8 C 1s peak can be deconvoluted into four sub-peaks at 284.0, 284.8, 285.7, and 289.1 eV, corresponding to sp^2 (56 at. %), sp^3 (17 at. %), C–(O,N) (21 at. %), and C=O (7 at. %) groups, respectively (Figure 3b). We observed that the C 1s of CMS-*c* was also a convolution of four sub-peaks at 284.7, 285.0, 285.7, and 289.0 eV, corresponding to sp^2 (40 at. %), sp^3 (28 at. %), C–(O,N) (24 at. %), and C=O (8 at. %) functionalities, respectively (Figure S10). Interestingly, the relative ratio of sp^2 carbons is significantly lower in CMS-*c* than in CMS-8, while the relative ratio of sp^3 carbons is much higher. This result demonstrated that benzoxazole rings lead to a higher relative ratio of sp^2 carbons following carbonization

https://doi.org/10.1021/acsanm.3c02516
ACS Appl. Nano Mater. 2023, 6, 14957–14966

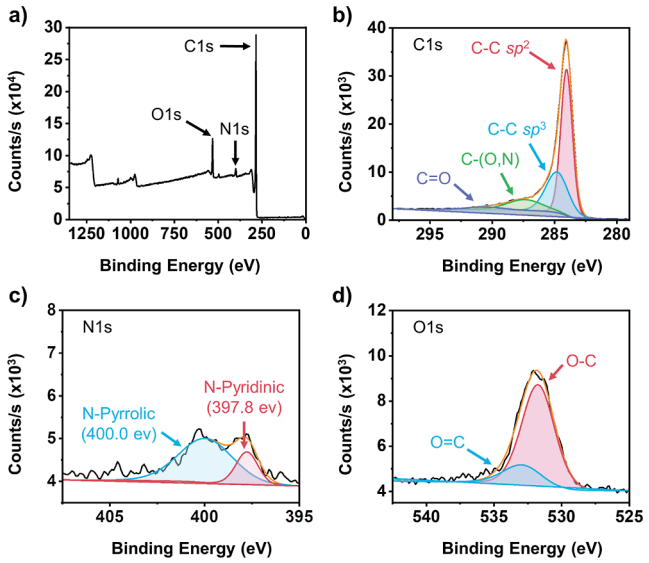

Figure 3. CMS XPS results. (a) Example XPS survey spectra of CMS-8. (b–d) High-resolution C 1s (b), N 1s (c), and O 1s (d) XPS spectra of CMS-8.

when compared to imide rings. Additionally, a higher sp^2/sp^3 ratio is also found in CMS-8 (4.67) when compared to CMS-*c* (1.45), which is also attributed to the benzoxazole ring structure in the TR-PBOx precursor (Table S2). As anticipated, the relative ratio of C−O/C−N is higher in CMS-*c* as more C−O/C−N bonds are observed in the molecular structure of the control IO precursor, while the relative ratio of C═O is similar for both CMS-*c* and CMS-8 (Figure 1).

N 1s peak of CMS-8 is a convolution of two sub-peaks at 400.0 and 397.8 eV, associated with 23 at. % of pyrrolic/pyridonic and 77 at. % of pyridinic nitrogen group types, respectively (Figure 3c). As a comparison, the CMS-*c* can also be deconvoluted into two sub-peaks at 401.2 and 398.3 eV, corresponding to pyrrolic/pyridonic (25 at. %) and pyridinic N (75 at. %) groups, respectively (Figure S10). Similar relative ratios were observed for both CMS-8 and CMS-*c*, which was anticipated because both precursors are composed of N-containing, heterocyclic ring structures with similar relative amount. However, a sharp difference was observed in the CMS-8 and CMS-*c* O 1s high-resolution scans. CMS-8 O 1s scans indicated the presence of two different bonding environments represented by peaks at 532.8 and 532.3 eV, corresponding to C═O (18 at. %) and C−O (82 at. %) functionalities, respectively (Figure 3d). CMS-*c* O 1s scans indicated the presence of the same bonding environments with sub-peaks at 532.3 and 532.7 eV, corresponding to C═O (84 at. %) and C−O (16 at. %) functionalities, respectively (Figure S10). Based on the molecular structure, a relative ratio of 4:1 (C−O/C═O) is expected for CMS-8, namely, due to the benzoxazole ring structure in TR-PBOx. The relative ratio of C−O/C═O is 4.5:1 in the CMS-8, which not only confirms that TR occurred, but also demonstrates the enhanced stability of the benzoxazole ring structure. A relative ratio of 5:9 (C−O/C═O) is expected for CMS-*c* based on the molecular structure of the IO precursor; however, a relative ratio closer to 1:5 (C−O/C═O) was observed in the CMS-*c*. The difference in relative ratio suggests that bond cleavage may occur at the ether C−O bonds in the IO network precursor, while imide carbonyls are maintained through carbonization.

All CMS derived from TR-PBOx had similar chemical compositions and sp^2/sp^3 ratios according to XPS characterization (Table S2). It is noteworthy that the atomic percentage of C increases as the oHIO precursor DP increases for CMS-4 (84.9%), CMS-8 (87.7%), and CMS-12 (89.1%). The crosslinking density can decrease as DP increases for PEPA end-capped IOs, which causes the compositional change in the final carbons.[36,63] The CMS-12 C composition becomes more comparable to linear polyimides (93.1%) that were carbonized up to 800 °C due to the decrease in the crosslinking density.[19]

CMS PSD and Structure. CMS pore volumes, surface areas, and PSDs were characterized by N_2 gas physisorption at 77 K. All CMS samples, including the non-TR IO-derived CMS (CMS-*c*), exhibited type I isotherms, which indicated the presence of microporosity (Figure 5a). Micropores in CMS-*c* are attributed to the asymmetric and fluorinated molecular structure in the IO backbone, which can hinder the tight packing of formed carbon strands leading to microporous CMS.[19,64,65] However, the BET surface area and pore volume of CMS-*c* (356 m^2/g, 0.124 cm^3/g) were much lower than the those of CMS derived from precursors that underwent TR conversion prior to carbonization. CMS-4 (667 m^2/g, 0.236 cm^3/g), CMS-8 (700 m^2/g, 0.244 cm^3/g), and CMS-12 (775 m^2/g, 0.283 cm^3/g) were observed to have nearly double the BET surface area and pore volume compared to CMS-*c*, demonstrating the beneficial impact of TR on pore formation of TR-PBOx-derived carbons (Table S2). PSDs were obtained using the HK method, assuming a slit-pore structure to probe the micropore size (Figure 5b).[66] CMS-*c* was observed to have a narrow PSD centered around 7.7 Å, which is similar to previous work studying the carbonization of linear polyimides with asymmetric backbones, containing a bimodal PSD with pore populations of 5.2 and 7.9 Å.[19] CMS-4, -8, and -12 were observed to have more narrow PSD between 6 and 7 Å, suggesting uniform micropores centered around 6.46, 6.61, and 6.40 Å, respectively. Micropore uniformity was attributed to the dense polymer network formed during end-capped, crosslinking and cyclization of PEPA, thus concentrating pore formation between the crosslinkers during TR and reducing defects during subsequent carbonization (Figure 4).

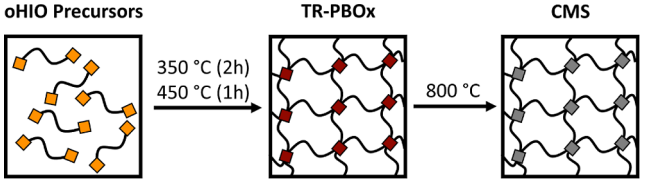

Figure 4. Idealized network formation of PEPA end-capped oHIO crosslinking and thermally rearranging into TR-PBOx intermediates between 350 and 450 °C, prior to being carbonized up to 800 °C, creating controlled micropore formation between 6 and 7 Å.

The CMS pore size was observed to be larger than previously studied linear fluorinated polyimide-derived CMSs (~5.5 Å), suggesting synergistic pore widening by combining a variety of molecular functionalities into the IO backbone, such as asymmetry, fluorination, and TR motifs.[64,65] It is worth noting that the CMSs exhibited similar pore sizes when carbonized at higher temperatures, such as 1000 and 1200 °C (Figure S13). Specifically, CMS-8 was carbonized at 1000 and 1200 °C

https://doi.org/10.1021/acsanm.3c02516
ACS Appl. Nano Mater. 2023, 6, 14957−14966

leading to pore sizes centered around 6.6−6.7 Å. However, CMS-8 pore surface area and volume were observed to decrease when carbonized at 1000 °C (571 m^2/g, 0.195 cm^3/g) and 1200 °C (558 m^2/g, 0.200 cm^3/g) (Table S3).

While narrow PSDs (6−7 Å) were observed for the CMS samples, PSD broadening was also noted as the oHIO precursor DP increased. Therefore, TR-PBOx films were prepared to elucidate the influence of polymer network density and FFV on the PSD, surface area, and pore volume of derived CMS. It was found that TR-PBOx film density decreased from 1.40 to 1.21 g/cm^3 as the oHIO precursor DP increased, suggesting a decrease in the crosslinking density, similar to previous reports (Table 1).[36,63] Decreasing crosslinking density

Table 1. Density and FFV of Crosslinked TR-PBOx Films

film precursor	density (g/cm^3)	FFV (%)
Control	1.35 ± 0.02	11.5 ± 0.9
oHIO-4	1.40 ± 0.03	14.0 ± 0.4
oHIO-8	1.39 ± 0.01	15.8 ± 0.6
oHIO-12	1.21 ± 0.01	26.7 ± 0.8

could explain the PSD broadening in CMS-8 and CMS-12. An inverse relationship between TR-PBOx film density and FFV was also observed, further confirming a decrease in the crosslinking density as the oHIO DP increases. The FFV of TR-PBOx films correlated well with the CMS pore surface area and volume changes, indicating a direct relationship between the TR-PBOx FFV and CMS microporosity.

WAXS characterization was performed to elucidate the CMS nanostructures. Intensity versus scattering vector (Q) plots in the log−log scale are shown in Figure 5c, wherein a Q^{-D} dependency was observed in the intermediate Q range (0.4−1.0 $Å^{-1}$) for all CMS samples. The fractal dimension (D) was measured to be between 2 and 2.5 for all CMS samples, suggesting the formation of planar slit micropores with bent (D = 2) or crumpled (D = 2.5) lamellae structures.[67] D values of CMS-c (2.0), CMS-4 (1.9), CMS-8 (2.2), and CMS-12 (2.1) were very similar, indicating consistent formation of bent lamellae structures.

Correlation size can be further characterized via a Kratky plot, wherein $I(Q)\bullet Q^2$ is plotted versus Q (Figure 5d). For clarity, $I(Q)$ is the intensity as a function of the X-ray scattering vector Q. The first peak at a Q of ∼0.4 $Å^{-1}$ is attributed to the micropores measured in gas physisorption, where domain spacing of the pore (d_p) were calculated for CMS-c (23.5 Å), CMS-4 (18.4 Å), CMS-8 (18.8 Å), and CMS-12 (19.3 Å) using Bragg's equation. Pore wall thickness was then extracted for CMS-c (15.8 Å), CMS-4 (12.0 Å), CMS-8 (12.2 Å), and CMS-12 (12.9 Å) by comparing PSD from gas physisorption characterization and calculated d_p.

The peak at Q of ∼1.6−1.7 $Å^{-1}$ was attributed to the carbon−carbon layer distances (d_c) and was calculated for CMS-c (3.7 Å), CMS-4 (3.7 Å), CMS-8 (3.6 Å), and CMS-12 (3.6 Å). These d_c values are higher than the ideal length of a single graphene layer (3.4 Å), suggesting that the resulting carbon has a disordered structure, which agrees well with the low sp^2/sp^3 ratios observed for CMS samples in the XPS characterization.

CO_2 sorption performance was characterized to demonstrate the practical application of the CMS. Previous literature has determined that a molecular sieving capability of >2 mmol of CO_2/g of sorbent is ideal for CO_2 adsorption applications.[68] In

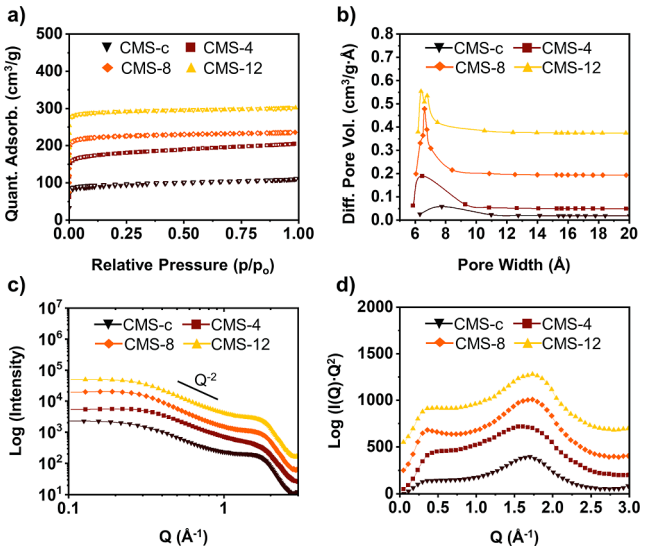

Figure 5. (a) Gas physisorption isotherms measured with N_2 at 77 K, which have been shifted in the positive Y-direction: CMS-c (+0), CMS-4 (+5), CMS-8 (+50), and CMS-12 (+150). Closed symbols signify adsorption, and open symbols signify desorption. (b) Differential pore volume plots measured using the HK method, which have been shifted in the positive Y-direction: CMS-c (+0.02), CMS-4 (+0.05), CMS-8 (+0.2), and CMS-12 (+0.4). (c) WAXS intensity profiles for CMS-c, CMS-4, CMS-8, and CMS-12, which have been shifted in the positive Y-direction: CMS-c (×1), CMS-4 (×1.5), CMS-8 (×3.5), and CMS-12 (×10). (d) Kratky plots for CMS-c, CMS-4, CMS-8, and CMS-12, which have been shifted in the positive Y-direction: CMS-c (+0), CMS-4 (+50), CMS-8 (+250), and CMS-12 (+550).

this investigation, CMS-8 (3.17 mmol of CO_2/g of CMS) and CMS-12 (3.12 mmol of CO_2/g of CMS) had the highest CO_2 sorption performances, while CMS-4 (3.08 mmol of CO_2/g of CMS) showed slightly lower sorption performance (Figure S14). However, it is worth noting that even CMS-c (2.42 mmol of CO_2/g of CMS) had great CO_2 sorption performance greatly exceeding the literature value of desired CO_2 capacity (>2 mmol of CO_2/g of sorbent).[68] The excellent CO_2 adsorption capabilities suggest the potential of the CMS for sorption and separation of other small molecules such as ethylene and xylene.

Fine-tuning the CMS Pore Size, Surface Area, and Volume. Mixing IO precursors could further provide the ability to tune the CMS pore size, surface area, and volume, thus allowing controlled molecular sieving separation capabilities. Therefore, oHIO-8 and the control samples were mixed in THF solutions at varying weight ratios to investigate the impact of composition on the porosity of mixed CMSs (mCMSs). All mixtures were thoroughly dried for 24 h at 250 °C under vacuum, removing all solvent residues before carbonization at 1 °C/min from 450 to 800 °C. Complete carbonization was confirmed via ATR−FTIR (Figure S8). It should be noted that oHIO-8 was selected in this study for solubility purposes. oHIO-12 had limited solubility in THF, despite CMS-12 having the highest BET surface area. All mCMSs were characterized using gas physisorption and WAXS measurements. mCMS samples were named according to CMS-c to oHIO-8 weight ratio. For example, mCMS 80:20 would indicate 80 wt % control to 20 wt % oHIO-8.

Type I isotherms were observed for all mCMSs, indicating that the microporosity was maintained after carbonizing of the

https://doi.org/10.1021/acsanm.3c02516
ACS Appl. Nano Mater. 2023, 6, 14957−14966

mixed precursors from blending the control and oHIO-8 (Figure 6a). BET surface area and pore volume for mCMS

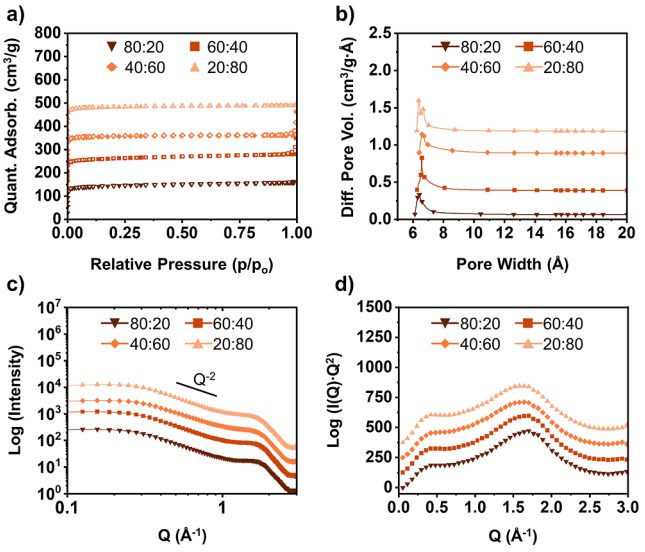

Figure 6. (a) Gas physisorption isotherms measured with N_2 at 77 K, which have been shifted in the positive *Y*-direction: 80:20 (+0), 60:40 (+100), 40:60 (+200), and 20:80 (+300). Closed symbols signify adsorption, and open symbols signify desorption. (b) Differential pore volume plots measured using HK method, which have been shifted in the positive *Y*-direction: CMS-*c* (+0.064), CMS-4 (+0.38), CMS-8 (+0.89), and CMS-12 (+1.2). (c) WAXS intensity profiles for mCMS 80:20, 60:40, 40:60, and 20:80, which have been shifted in the positive *Y*-direction: CMS-*c* (×0.1), CMS-4 (×0.5), CMS-8 (×1.5), and CMS-12 (×5.0). (d) Kratky plots for mCMS 80:20, 60:40, 40:60, and 20:80, which have been shifted in the positive *Y*-direction: CMS-*c* (+0), CMS-4 (+125), CMS-8 (+250), and CMS-12 (+375).

80:20 (569 m^2/g, 0.220 cm^3/g), 60:40 (638 m^2/g, 0.222 cm^3/g), 40:60 (638 m^2/g, 0.221 cm^3/g), and 20:80 (735 m^2/g, 0.256 cm^3/g) increased as the control to oHIO-8 mass ratio decreased, suggesting that controlled pore surface area manipulation can be achieved by leveraging polymer precursor mixing (Table S4). Monomodal micropores were centered around 6−7 Å for mCMS 80:20 (6.4 Å), 60:40 (6.6 Å), 40:60 (6.6 Å), and 20:80 (6.4 Å) (Figure 6b).[66] Interestingly, micropores in mCMS were more uniform than CMS-8 alone, suggested by their narrower PSD, most notably in mCMS 60:40. PSD narrowing was attributed to mixing the control precursor, which had a much lower FFV after crosslinked network formation than the oHIO-8 precursor. Uniform mCMS PSD results suggested that FFV, ergo crosslinking density, plays a significant role in CMS pore formation, demonstrating the importance of oligomer molecular design considerations when preparing CMS for molecular sorption and separation applications.

WAXS characterization was employed to determine the nanostructure changes of samples upon conversion to mCMS from polymer precursor. Intensity versus *Q* plots in the log−log scale are shown in Figure 6c, wherein a Q^{-1} dependency was found in the intermediate *Q* range (0.4−1.0 $Å^{-1}$) for all mCMS samples.

D values of mCMS 80:20 (2.0), 60:40 (2.0), 40:60 (1.9), and 20:80 (2.0) indicate that bent lamellae structures were maintained in mCMS, while the changes in pore size, surface area, and volume were observed. Correlation size was characterized via a Kratky plot, wherein two local *Q* maximum values were observed (Figure 6d).The first peak at a *Q* value of 0.4 $Å^{-1}$ is attributed to the micropores measured in gas physisorption, where d_p was calculated to be similar for mCMS 80:20 (19.5 Å), 60:40 (19.0 Å), 40:60 (18.9 Å), and 20:80 (18.3 Å). Pore wall thickness was determined, including mCMS 80:20 (13.1 Å), 60:40 (12.4 Å), 40:60 (12.3 Å), and 20:80 (11.9 Å) in which pore wall thickness decreased at larger concentrations of the oHIO-8 precursor.

Collectively, these results demonstrate that both backbone chemistry and polymer network architecture of oligomer precursors play essential roles in controlling the pore formation of final CMS. Using different molecular designs, CMS porosity could be fine-tuned to match the specific molecular sorption and separation requirements, further expanding CMS utilization. Therefore, it is important to continue to explore different backbone chemistries and polymer network architectures to further improve future molecular sorption and separation capabilities.

CONCLUSIONS

This study demonstrated that controlled CMS microporosity could be achieved through molecular engineering of oligomer precursor backbone chemistry and polymer network architecture. Rational design of end-capped crosslinking oHIO precursors, with TR functionalities and asymmetric molecular structures between the crosslinks, provides an avenue for preparing CMS with well-defined, planar slit micropores between 6 and 7 Å, BET surface areas up to 775 m^2/g, and CO_2 sorption performance up to 3.17 mmol of CO_2/g. Furthermore, this research demonstrated that CMS microporosity could be further tailored by blending different precursors with varying FFV, forming mCMS with adjustable pore size (6.4−6.6 Å) and BET surface area (569−735 m^2/g). Potential research opportunities exist for preparing CMS membranes from oHIO precursors and characterizing the CMS membranes to understand their molecular sieving properties, as well as fabricating microporous fibers with well-defined sub-nm pore sizes due to the excellent solubility of oHIO precursors.

ASSOCIATED CONTENT

Supporting Information

The Supporting Information is available free of charge at https://pubs.acs.org/doi/10.1021/acsanm.3c02516.

Synthesis of oHIOs; preparation of TR-PBOx films; solution-state ^1H NMR spectra for the control, oHIO-4, oHIO-8, and oHIO-12; TGA-MS thermogram for oHIO-4; solid-state CP-MAS ^{13}C NMR spectra for the control and oHIO-4; ATR−FTIR spectra for CMS samples and mixtures; SEM images of CMS-*c* and CMS-8; XPS spectra for CMS-*c*, CMS-4, and CMS-12; N_2 gas physisorption isotherms and X-ray spectra for oHIO-8 carbonized at 800, 1000, and 1200 °C; CO_2 gas physisorption isotherms for CMS-*c*, CMS-4, and CMS-12; oHIO precursor GPC data; CMS pore properties and chemical composition; pore properties for CMS-8 carbonized at 1000 and 1200 °C; and references(PDF)

AUTHOR INFORMATION

Corresponding Author

Jeffrey S. Wiggins − *School of Polymer Science & Engineering, University of Southern Mississippi, Hattiesburg, Mississippi*

https://doi.org/10.1021/acsanm.3c02516
ACS Appl. Nano Mater. 2023, 6, 14957−14966

39406, United States; orcid.org/0000-0001-7662-0669; Email: Jeffrey.Wiggins@usm.edu

Authors

William Guzman − *School of Polymer Science & Engineering, University of Southern Mississippi, Hattiesburg, Mississippi 39406, United States;* orcid.org/0000-0002-6309-4601

Anthony Griffin − *School of Polymer Science & Engineering, University of Southern Mississippi, Hattiesburg, Mississippi 39406, United States;* orcid.org/0000-0003-0526-194X

Mark Robertson − *School of Polymer Science & Engineering, University of Southern Mississippi, Hattiesburg, Mississippi 39406, United States*

William L. Jarrett − *School of Polymer Science & Engineering, University of Southern Mississippi, Hattiesburg, Mississippi 39406, United States*

Zhe Qiang − *School of Polymer Science & Engineering, University of Southern Mississippi, Hattiesburg, Mississippi 39406, United States;* orcid.org/0000-0002-3539-9053

Complete contact information is available at: https://pubs.acs.org/10.1021/acsanm.3c02516

Author Contributions

The manuscript was written through contributions of all authors. All authors have given approval to the final version of the manuscript.

Funding

This research was funded by the US Army Research Laboratory (Award W911NF-18-2-0061). A.G., M.R. and Z.Q. acknowledge the support from the National Science Foundation (CMMI-2239408). The purchase of the XPS instrumentation used in this work was supported by the NSF Major Research Instrumentation program (DMR-1726901). The authors would like to thank the support from the University of Southern Mississippi.

Notes

The authors declare no competing financial interest.

■ ACKNOWLEDGMENTS

The authors gratefully acknowledge the support of this research from Dr. John La Scala of the US Army Research Laboratory (Award W911NF-18-2-0061). The authors would like to thank Dr. Xiaodan Gu and Guorong Ma from the University of Southern Mississippi (USM) for assisting with WAXS experiments. Additionally, the authors would like to thank Dr. Derek Patton and Surabhi Jha from USM for assisting with XPS experiments. The authors are also grateful to Dr. Jin Gyu Park and Dr. Richard Liang from the High-Performance Materials Institute at Florida-State University for assisting with SEM imaging. The authors would further like to thank Dr. Vinay Mishra and Dr. Jeff Dimmit from Jayhawk Fine Chemicals Corporation (part of CABB Group GmbH) for material donations. Furthermore, the authors are appreciative to Henrik Bernquist and Borys Schafran from Nexam Chemical for material donations. Lastly, the authors are grateful for the donation of the Thermalimide film from Alex Dahlgren and Sissi Lopez from Airtech Advance Materials Group.

■ REFERENCES

(1) Sazali, N. A Review of the Application of Carbon-Based Membranes to Hydrogen Separation. *J. Mater. Sci.* **2020**, *55*, 11052−11070.

(2) Wang, Y.; Ghanem, B. S.; Ali, Z.; Hazazi, K.; Han, Y.; Pinnau, I. Recent Progress on Polymers of Intrinsic Microporosity and Thermally Modified Analogue Materials for Membrane-Based Fluid Separations. *Small Struct.* **2021**, *2*, 2170026.

(3) Sholl, D. S.; Lively, R. P. Seven Chemical Separations to Change the World. *Nature* **2016**, *532*, 435−437.

(4) Bernardo, P.; Drioli, E.; Golemme, G. Membrane Gas Separation: A Review/State of the Art. *Ind. Eng. Chem. Res.* **2009**, *48*, 4638−4663.

(5) Ren, Y.; Liang, X.; Dou, H.; Ye, C.; Guo, Z.; Wang, J.; Pan, Y.; Wu, H.; Guiver, M. D.; Jiang, Z. Membrane-Based Olefin/Paraffin Separations. *Adv. Sci.* **2020**, *7*, 2001398.

(6) Koros, W. J.; Zhang, C. Materials for Next-Generation Molecularly Selective Synthetic Membranes. *Nat. Mater.* **2017**, *16*, 289−297.

(7) Du, S.; Huang, J.; Ryder, M. R.; Daemen, L. L.; Yang, C.; Zhang, H.; Yin, P.; Lai, Y.; Xiao, J.; Dai, S.; Chen, B. Probing Sub-5 Ångstrom Micropores in Carbon for Precise Light Olefin/Paraffin Separation. *Nat. Commun.* **2023**, *14*, 1197.

(8) Dong, Z.; Li, B.; Shang, H.; Zhang, P.; Chen, S.; Yang, J.; Zeng, Z.; Wang, J.; Deng, S. Ultramicroporous Carbon Granules with Narrow Pore Size Distribution for Efficient CH_4 Separation from Coal-bed Gases. *AIChE J.* **2021**, *67*, No. e17281.

(9) Zhao, Z.; Wu, K.; Peng, Y.; Liu, Y.; Deng, Z.; Han, X.; Chen, S.; Chen, J.; Deng, S.; Wang, J. Microporous Carbon Granules with Narrow Pore Size Distribution and Rich Oxygen Functionalities for Xe/Kr Separation. *Sep. Purif. Technol.* **2022**, *302*, 122074.

(10) Zhao, Z.; Liu, Y.; Liu, X.; Liu, Y.; Chen, J.; Chen, S.; Deng, S.; Wang, J. One-step Purification of Ethylene from Acetylene and Carbon Dioxide by Ultramicroporous Carbons. *AIChE J.* **2023**, *69*, No. e18046.

(11) Zhang, P.; Wang, J.; Fan, W.; Zhong, Y.; Zhang, Y.; Deng, Q.; Zeng, Z.; Deng, S. Ultramicroporous Carbons with Extremely Narrow Pore Size Distribution via In-Situ Ionic Activation for Efficient Gas-Mixture Separation. *Chem. Eng. J.* **2019**, *375*, 121931.

(12) Modak, A.; Bhaumik, A. Porous Carbon Derived via KOH Activation of a Hypercrosslinked Porous Organic Polymer for Efficient CO2, CH4, H2 Adsorptions and High CO2/N2 Selectivity. *J. Solid State Chem.* **2015**, *232*, 157−162.

(13) EL-Mahdy, A. F. M.; Young, C.; Kim, J.; You, J.; Yamauchi, Y.; Kuo, S.-W. Hollow Microspherical and Microtubular [3 + 3] Carbazole-Based Covalent Organic Frameworks and Their Gas and Energy Storage Applications. *ACS Appl. Mater. Interfaces* **2019**, *11*, 9343−9354.

(14) EL-Mahdy, A. F. M.; Kuo, C.-H.; Alshehri, A.; Young, C.; Yamauchi, Y.; Kim, J.; Kuo, S.-W. Strategic Design of Triphenylamine- and Triphenyltriazine-Based Two-Dimensional Covalent Organic Frameworks for CO2 Uptake and Energy Storage. *J. Mater. Chem. A* **2018**, *6*, 19532−19541.

(15) Zhang, S.; Yang, Q.; Wang, C.; Luo, X.; Kim, J.; Wang, Z.; Yamauchi, Y. Porous Organic Frameworks: Advanced Materials in Analytical Chemistry. *Adv. Sci.* **2018**, *5*, 1801116.

(16) Chaikittisilp, W.; Hu, M.; Wang, H.; Huang, H.-S.; Fujita, T.; Wu, K. C.-W.; Chen, L.-C.; Yamauchi, Y.; Ariga, K. Nanoporous Carbons through Direct Carbonization of a Zeolitic Imidazolate Framework for Supercapacitor Electrodes. *Chem. Commun.* **2012**, *48*, 7259−7261.

(17) Wang, C.; Kim, J.; Tang, J.; Kim, M.; Lim, H.; Malgras, V.; You, J.; Xu, Q.; Li, J.; Yamauchi, Y. New Strategies for Novel MOF-Derived Carbon Materials Based on Nanoarchitectures. *Chem* **2020**, *6*, 19−40.

(18) Qiu, W.; Leisen, J. E.; Liu, Z.; Quan, W.; Koros, W. J. Key Features of Polyimide-Derived Carbon Molecular Sieves. *Angew. Chem., Int. Ed.* **2021**, *60*, 22322−22331.

(19) Liu, Z.; Qiu, W.; Quan, W.; Koros, W. J. Advanced Carbon Molecular Sieve Membranes Derived from Molecularly Engineered Cross-Linkable Copolyimide for Gas Separations. *Nat. Mater.* **2023**, *22*, 109−116.
(20) Yang, Y.; He, Z.; Liu, Y.; Wang, S.; Wang, H.; Zhu, G. Facile Preparation of N-Doped Hierarchically Porous Carbon Derived from Pitch-Based Hyper-Cross-Linked Polymers as an Efficient Metal-Free Catalyst for Oxygen-Reduction. *Appl. Surf. Sci.* **2021**, *565*, 150579.
(21) Luo, J.; Zhang, H.; Zhang, Z.; Yu, J.; Yang, Z. In-Built Template Synthesis of Hierarchical Porous Carbon Microcubes from Biomass toward Electrochemical Energy Storage. *Carbon* **2019**, *155*, 1−8.
(22) Ma, Y.; Bruno, N. C.; Zhang, F.; Finn, M. G.; Lively, R. P. Zeolite-like Performance for Xylene Isomer Purification Using Polymer-Derived Carbon Membranes. *Proc. Natl. Acad. Sci. U.S.A.* **2021**, *118*, No. e2022202118.
(23) Koh, D.-Y.; McCool, B. A.; Deckman, H. W.; Lively, R. P. Reverse Osmosis Molecular Differentiation of Organic Liquids Using Carbon Molecular Sieve Membranes. *Science* **2016**, *353*, 804−807.
(24) Fahim, M. A.; Alsahhaf, T. A.; Elkilani, A. S. *Fundamentals of Petroleum Refining*, 1st ed.; Elsevier: Amsterdam, 2010.
(25) Yang, Y.; Bai, P.; Guo, X. Separation of Xylene Isomers: A Review of Recent Advances in Materials. *Ind. Eng. Chem. Res.* **2017**, *56*, 14725−14753.
(26) Yoon, Y. H.; Lively, R. P. Co-Transport of Water and p-Xylene through Carbon Molecular Sieve Membranes. *J. Membr. Sci.* **2022**, *654*, 120495.
(27) Ma, Y.; Jue, M. L.; Zhang, F.; Mathias, R.; Jang, H. Y.; Lively, R. P. Creation of Well-Defined "Mid-Sized" Micropores in Carbon Molecular Sieve Membranes. *Angew. Chem., Int. Ed.* **2019**, *58*, 13259−13265.
(28) Low, Z.-X.; Budd, P. M.; McKeown, N. B.; Patterson, D. A. Gas Permeation Properties, Physical Aging, and Its Mitigation in High Free Volume Glassy Polymers. *Chem. Rev.* **2018**, *118*, 5871−5911.
(29) Tullos, G. L.; Powers, J. M.; Jeskey, S. J.; Mathias, L. J. Thermal Conversion of Hydroxy-Containing Imides to Benzoxazoles: Polymer and Model Compound Study. *Macromolecules* **1999**, *32*, 3598−3612.
(30) Park, H. B.; Jung, C. H.; Lee, Y. M.; Hill, A. J.; Pas, S. J.; Mudie, S. T.; Van Wagner, E.; Freeman, B. D.; Cookson, D. J. Polymers with Cavities Tuned for Fast Selective Transport of Small Molecules and Ions. *Science* **2007**, *318*, 254−258.
(31) Calle, M.; Doherty, C. M.; Hill, A. J.; Lee, Y. M. Cross-Linked Thermally Rearranged Poly(Benzoxazole- *Co* -Imide) Membranes for Gas Separation. *Macromolecules* **2013**, *46*, 8179−8189.
(32) Smith, Z. P.; Hernández, G.; Gleason, K. L.; Anand, A.; Doherty, C. M.; Konstas, K.; Alvarez, C.; Hill, A. J.; Lozano, A. E.; Paul, D. R.; Freeman, B. D. Effect of Polymer Structure on Gas Transport Properties of Selected Aromatic Polyimides, Polyamides and TR Polymers. *J. Membr. Sci.* **2015**, *493*, 766−781.
(33) Han, S. H.; Misdan, N.; Kim, S.; Doherty, C. M.; Hill, A. J.; Lee, Y. M. Thermally Rearranged (TR) Polybenzoxazole: Effects of Diverse Imidization Routes on Physical Properties and Gas Transport Behaviors. *Macromolecules* **2010**, *43*, 7657−7667.
(34) Han, S. H.; Kwon, H. J.; Kim, K. Y.; Seong, J. G.; Park, C. H.; Kim, S.; Doherty, C. M.; Thornton, A. W.; Hill, A. J.; Lozano, Á. E.; Berchtold, K. A.; Lee, Y. M. Tuning Microcavities in Thermally Rearranged Polymer Membranes for CO2 Capture. *Phys. Chem. Chem. Phys.* **2012**, *14*, 4365.
(35) Do, Y. S.; Lee, W. H.; Seong, J. G.; Kim, J. S.; Wang, H. H.; Doherty, C. M.; Hill, A. J.; Lee, Y. M. Thermally Rearranged (TR) Bismaleimide-Based Network Polymers for Gas Separation Membranes. *Chem. Commun.* **2016**, *52*, 13556−13559.
(36) Hergenrother, P. M.; Connell, J. W.; Smith, J. G. Phenylethynyl Containing Imide Oligomers. *Polymer* **2000**, *41*, 5073−5081.
(37) Hergenrother, P. M.; Smith, J. G. Chemistry and Properties of Imide Oligomers End-Capped with Phenylethynylphthalic Anhydrides. *Polymer* **1994**, *35*, 4857−4864.
(38) Xu, X.; Liu, Y.; Lan, B.; Mo, S.; Zhai, L.; He, M.; Fan, L. High Thermally Stable and Melt Processable Polyimide Resins Based on Phenylethynyl-Terminated Oligoimides Containing Siloxane Structure. *Materials* **2020**, *13*, 3742.
(39) Connell, J. W.; Smith, J. G.; Hergenrother, P. M. Oligomers and Polymers Containing Phenylethynyl Groups. *J. Macromol. Sci., Part C: Polym. Rev.* **2000**, *40*, 207−230.
(40) Miyauchi, M.; Ishida, Y.; Ogasawara, T.; Yokota, R. Novel Phenylethynyl-Terminated PMDA-Type Polyimides Based on KAPTON Backbone Structures Derived from 2-Phenyl-4,4′-Diaminodiphenyl Ether. *Polym. J.* **2012**, *44*, 959−965.
(41) Li, X.; Miyauchi, M.; González, C.; Nutt, S. Thermal Oxidation of PEPA-Terminated Polyimide. *High Perform. Polym.* **2019**, *31*, 707−718.
(42) Zhang, Y.; Jain, A.; Grunenfelder, L. K.; Miyauchi, M.; Nutt, S. Process Development for Phenylethynyl-Terminated PMDA-Type Asymmetric Polyimide Composites. *High Perform. Polym.* **2018**, *30*, 731−741.
(43) Cho, D.; Drzal, L. T. *FT-IR Studies on Imidization and End Group Reaction Behaviors of a Phenylethynyl Terminated Imide Oligomer*; ICCM 12 Conference Proceedings: Paris, 1999; p 10.
(44) Wang, P.; Liu, M.; Ran, Q. The Study on Curing and Weight-Loss Mechanisms of Benzoxazine during Thermal Curing Process. *Polym. Degrad. Stab.* **2020**, *179*, 109279.
(45) Bryant, R. G. Polyimides. In *Encyclopedia of Polymer Science and Technology*; John Wiley & Sons, Inc.: Hoboken, NJ, USA, 2006; p pst272.pub2.
(46) Liu, C.; Zhao, X.; Yu, X.; Wang, W.; Jia, H.; Li, Y.; Zhou, H.; Chen, C. A Study of the Thermal Cure of New Trifunctional Phenylethynyl Terminated Imide Oligomers with Reduced Cure Temperatures. *Polym. Degrad. Stab.* **2013**, *98*, 230−240.
(47) Takekoshi, T.; Terry, J. M. High-Temperature Thermoset Polyimides Containing Disubstituted Acetylene End Groups. *Polymer* **1994**, *35*, 4874−4880.
(48) Holland, T. V.; Glass, T. E.; McGrath, J. E. Investigation of the Thermal Curing Chemistry of the Phenylethynyl Group Using a Model Aryl Ether Imide. *Polymer* **2000**, *41*, 4965−4990.
(49) Guzman, W.; Johnson, I.; Wiggins, J. S. Thermal Rearrangement Conversion of Cross-Linked *Ortho* -Hydroxy Polyimide Networks. *ACS Appl. Polym. Mater.* **2022**, *4*, 7135−7143.
(50) Li, X.; Liu, T.; Jiao, Y.; Dong, J.; Gan, F.; Zhao, X.; Zhang, Q. Novel High-Performance Poly(Benzoxazole-Co-Imide) Resins with Low Dielectric Constants and Superior Thermal Stabilities Derived from Thermal Rearrangement of Ortho-Hydroxy Polyimide Oligomers. *Chem. Eng. J.* **2019**, *359*, 641−651.
(51) Li, X.; Zhang, P.; Dong, J.; Gan, F.; Zhao, X.; Zhang, Q. Preparation of Low-κ Polyimide Resin with Outstanding Stability of Dielectric Properties versus Temperature by Adding a Reactive Cardo-Containing Diluent. *Composites, Part B* **2019**, *177*, 107401.
(52) Schaefer, J.; Stejskal, E. O.; Buchdahl, R. Magic-Angle ^{13}C NMR Analysis of Motion in Solid Glassy Polymers. *Macromolecules* **1977**, *10*, 384−405.
(53) Metz, G.; Wu, X. L.; Smith, S. O. Ramped-Amplitude Cross Polarization in Magic-Angle-Spinning NMR. *J. Magn. Reson., Ser. A* **1994**, *110*, 219−227.
(54) Wu, A. X.; Lin, S.; Mizrahi Rodriguez, K.; Benedetti, F. M.; Joo, T.; Grosz, A. F.; Storme, K. R.; Roy, N.; Syar, D.; Smith, Z. P. Revisiting Group Contribution Theory for Estimating Fractional Free Volume of Microporous Polymer Membranes. *J. Membr. Sci.* **2021**, *636*, 119526.
(55) Li, S.; Dai, Z.; Wang, T.; Huang, Z.; Guo, R. Pentiptycene-Containing Polybenzoxazole Membranes with a Crosslinked Unimodal Network Structure for High-Temperature Hydrogen Separations. *Chem. Mater.* **2022**, *34*, 9577−9588.
(56) Guzman, W.; Johnson, I.; Wiggins, J. S. Thermal Rearrangement Conversion of Cross-Linked *Ortho* -Hydroxy Polyimide Networks. *ACS Appl. Polym. Mater.* **2022**, *4*, 7135−7143.
(57) Guo, R.; Sanders, D. F.; Smith, Z. P.; Freeman, B. D.; Paul, D. R.; McGrath, J. E. Synthesis and Characterization of Thermally Rearranged (TR) Polymers: Effect of Glass Transition Temperature

https://doi.org/10.1021/acsanm.3c02516
ACS Appl. Nano Mater. 2023, 6, 14957−14966

of Aromatic Poly(Hydroxyimide) Precursors on TR Process and Gas Permeation Properties. *J. Mater. Chem. A* **2013**, *1*, 6063.
(58) Smith, Z. P.; Czenkusch, K.; Wi, S.; Gleason, K. L.; Hernández, G.; Doherty, C. M.; Konstas, K.; Bastow, T. J.; Álvarez, C.; Hill, A. J.; Lozano, A. E.; Paul, D. R.; Freeman, B. D. Investigation of the Chemical and Morphological Structure of Thermally Rearranged Polymers. *Polymer* **2014**, *55*, 6649−6657.
(59) Ma, X.; Swaidan, R.; Teng, B.; Tan, H.; Salinas, O.; Litwiller, E.; Han, Y.; Pinnau, I. Carbon Molecular Sieve Gas Separation Membranes Based on an Intrinsically Microporous Polyimide Precursor. *Carbon* **2013**, *62*, 88−96.
(60) Salinas, O.; Ma, X.; Litwiller, E.; Pinnau, I. High-Performance Carbon Molecular Sieve Membranes for Ethylene/Ethane Separation Derived from an Intrinsically Microporous Polyimide. *J. Membr. Sci.* **2016**, *500*, 115−123.
(61) Hazazi, K.; Ma, X.; Wang, Y.; Ogieglo, W.; Alhazmi, A.; Han, Y.; Pinnau, I. Ultra-Selective Carbon Molecular Sieve Membranes for Natural Gas Separations Based on a Carbon-Rich Intrinsically Microporous Polyimide Precursor. *J. Membr. Sci.* **2019**, *585*, 1−9.
(62) Wang, H.; Shao, Y.; Mei, S.; Lu, Y.; Zhang, M.; Sun, J.; Matyjaszewski, K.; Antonietti, M.; Yuan, J. Polymer-Derived Heteroatom-Doped Porous Carbon Materials. *Chem. Rev.* **2020**, *120*, 9363−9419.
(63) Connell, J. W.; Hergenrother, P. M.; Hergenrother, P. M. The Effect of Phenylethynyl Terminated Imide Oligomer Molecular Weight on the Properties of Composites. *J. Compos. Mater.* **2000**, *34*, 614−628.
(64) Ohta, N.; Nishi, Y.; Morishita, T.; Tojo, T.; Inagaki, M. Preparation of Microporous Carbon Films from Fluorinated Aromatic Polyimides. *Carbon* **2008**, *46*, 1350−1357.
(65) Ohta, N.; Nishi, Y.; Morishita, T.; Tojo, T.; Inagaki, M. Water Vapour Adsorption of Microporous Carbon Films Prepared from Fluorinated Aromatic Polyimides. *Adsorpt. Sci. Technol.* **2008**, *26*, 373−382.
(66) Horváth, G.; Kawazoe, K. Method for the Calculation of Effective Pore Size Distribution in Molecular Sieve Carbon. *J. Chem. Eng. Jpn.* **1983**, *16*, 470−475.
(67) Saurel, D.; Segalini, J.; Jauregui, M.; Pendashteh, A.; Daffos, B.; Simon, P.; Casas-Cabanas, M. A SAXS Outlook on Disordered Carbonaceous Materials for Electrochemical Energy Storage. *Energy Storage Mater.* **2019**, *21*, 162−173.
(68) Patel, H. A.; Byun, J.; Yavuz, C. T. Carbon Dioxide Capture Adsorbents: Chemistry and Methods. *ChemSusChem* **2017**, *10*, 1303−1317.

https://doi.org/10.1021/acsanm.3c02516
ACS Appl. Nano Mater. 2023, 6, 14957−14966